The Astrophysical Journal, 682: L133–L136, 2008 August 1

CORRELATION BETWEEN THE SHARP VARIATION OF THE TRANSPORT RATE OF MAGNETIC HELICITY AND SOLAR ERUPTIVE EVENTS

Yin Zhang, Baolin Tan, and Yihua Yan
The National Astronomical Observatories, Chinese Academy of Sciences, Datun Road A20, Chaoyang District, Beijing 100012, China; zhangyin@bao.ac.cn
Received 2007 November 20; accepted 2008 June 11; published 2008 July 9

ABSTRACT

In this Letter we report a close relationship between the variations of the transport rate of magnetic helicity (*dH*/*dt*) and a microwave burst. The latter may be regarded as a prompt signal of nonthermal energetic particles originating from the magnetic reconnection during solar flaring events. We analyze the observations of magnetograms of MDI/*SOHO* and SOT/*Hinode* and the high-cadence microwave observation at 2.84 GHz obtained by the Chinese Solar Broadband Radiospectrometer (SBRS/*Huairou*) of a flare/CME event that occurred in NOAA Active Region 10930 on 2006 December 13. We find that there is a sharp jump of *dH*/*dt* around the onset and quench of a microwave burst at a frequency of 2.84 GHz: the rate of *dH*/*dt* changes from negative to positive around the start of the eruption and recovers to negative when the eruption stopped. Furthermore, the temporal profile of *dH*/*dt* is consistent with that of a microwave burst. These results indicate that sharp variations of *dH*/*dt* are closely related to the solar eruption.

Subject headings: Sun: activity — Sun: flares — Sun: magnetic fields

1. INTRODUCTION

It is generally believed that energy released in solar activities, such as flares and CMEs, is provided by the nonpotential component of the magnetic field. There are several parameters available, such as shear angle, longitudinal current density, and current helicity density, for the description of the nonpotentiality of the magnetic field. These parameters can be deduced from observations of photospheric vector magnetograms. To fully understand the process of magnetic energy storage and release during the period of solar eruption, one must know the evolution of these nonpotential characteristics. For several decades many people have investigated this topic (Lin & Gaizauskas 1987; Leka et al. 1996; Bao & Zhang 1998; Deng et al. 2001; Wang et al. 2004; Tan et al. 2006; and others). However, this topic is still an open question and is not settled.

Like the nonpotential parameters mentioned above, magnetic helicity is another quantitative measurement of the global chiral properties of the magnetic field. It is conserved in a closed volume, as well as in an open volume in the absence of boundary flows (Berger & Field 1984). As the solar corona is an open volume with the photosphere as a boundary with normal flux, the magnetic helicity can be transported across the boundary by the passage of helical field lines through the surface (the first term) or by the shuffling horizontal motion of field lines on the surface (the second term) (Berger & Field 1984):

$$\frac{dH}{dt} = \oint 2(\boldsymbol{B}\cdot\boldsymbol{A}_p)v_z dS - \oint 2(\boldsymbol{v}\cdot\boldsymbol{A}_p)B_z dS, \quad (1)$$

where $\boldsymbol{v}$ is the velocity computed by the tracking method, B_z is the normal component of magnetic field, and $\boldsymbol{A}_p$ is the magnetic vector potential, which is uniquely specified by the observed flux distribution on the surface with the equations

$$\nabla\times\boldsymbol{A}_p\cdot\hat{z} = B_z, \quad \nabla\cdot\boldsymbol{A}_p = 0, \quad \boldsymbol{A}_p\cdot\hat{z} = 0. \quad (2)$$

The second term of equation (1) has been observationally determined by Chae et al. (2001) from a time series of line-of-sight magnetograms with the local correlation tracking (LCT) method (November & Simon 1988). Démoulin & Berger (2003) realized that the helicity calculated with the LCT method yields not only the helicity injected from shearing motions but also the helicity coming from flux emergence. Recently, a series of works have pointed out that sudden changes of *dH*/*dt* are closely correlated with solar eruptive events, such as flares/CMEs as well as the formation of filaments (Moon et al. 2002a, 2002b, 2003; Maeshiro et al. 2005). However, Hartkorn & Wang (2004) have pointed out that the reversal effect that can disturb MDI magnetic field measurements may also lead to impulsive changes of *dH*/*dt* during the flaring time. Nevertheless, the result is still inconclusive. Further efforts are necessary to understand the relationships between *dH*/*dt* and solar eruptions.

On 2006 December 13, an X3.4 flare/CME event occurred in AR 10930. This active region is a unique AR on the solar disk when the flare took place, and it is the dominant AR during its solar disk passage. It is generally believed that a microwave burst is a prompt signal of nonthermal energetic particles originating from the magnetic reconnection, which is responsible for the solar eruption, such as flares and CMEs. So, we examine the temporal variation of *dH*/*dt* associated with a microwave burst at a frequency of 2.84 GHz during the flaring time. We organized our Letter as follows. Section 2 is a brief introduction of the data and method. Section 3 gives the observational results. The discussion and conclusion are presented in § 4.

2. DATE AND METHOD

According to Solar Geophysical Data information, AR 10930 was visible on the east limb of the solar disk as a β region with a large leading sunspot on 2006 December 6. It developed into a $\beta\gamma\delta$ region on December 7. There was a significant flux emergence in the following sunspot from December 10 to 13. Associated with the emergence, the following sunspot rotated counterclockwise around its center and moved eastward rapidly, resulting in an increase in magnetic complexity. Furthermore, the following sunspot rotated up to 240° around its center before the major flare (Zhang et al. 2007). This flare is a typical two-ribbon flare, which is associated with a halo CME.

We use 96 minute full-disk longitudinal magnetograms taken by the Michelson Doppler Imager on board the *Solar and Heliospheric Observatory* (MDI/*SOHO*) to calculate *dH*/*dt* during the AR solar disk passage from December 8 to December 14. There is evidently a Zeeman saturation effect in the sunspot umbral area for the MDI magnetogram (Berger & Lites 2003; Nindos et al. 2003). We carry out the LCT using the original MDI data, which gives the lower limit of the calculation. Moreover, the saturation is a long-term effect, while the changes we are interested in are only on a timescale of about 100 minutes. So we think its influence can be neglected. In addition, Qiu & Gary (2003) found a reversal effect in MDI data during the impulsive phase of the flare. In our work, the impulsive phase of the flare was during 02:21–02:40 UT. The data of 96 minute full-disk magnetograms before and after the flare was obtained at 01:39 and 03:15, respectively, which means that the reversal effect could be excluded.

We use 2 minute longitudinal magnetograms of the Solar Optical Telescope (SOT) (Tsuneta et al. 2008) on board *Hinode* (Kosugi et al. 2007) to study the temporal variation of *dH*/*dt* during the flaring time. SOT produces two kinds of polarimetric data for the measurement of magnetic fields on the Sun by two instruments: Stokes *I* and *V* images taken by the Narrowband Filter Imager (NFI) and spectral profiles of full Stokes parameters taken by the Spectro-polarimeter (SP). The narrowband filter of NFI/SOT was positioned at −120 mÅ of the Fe I 6302.5 Å line. We use a set of NFI/SOT data that were obtained from 01:00 UT to 05:00 UT on December 13. Chae et al. (2007) have calibrated the NFI/SOT data with respect to the field determined from the SP/SOT data and presented a nonlinear correlation formula in their paper. We follow them to calibrate the NFI/SOT data. Isobe et al. (2007) found that the sign reversal of the 6302 Å *V* count was cospatial and cotemporal with the flare ribbon in 6302 Å *I* during the impulsive phase of this flare. This means that the data of SOT suffer from the reversal effect. The gray-scale image in Figure 1 is a negative image of 6302 Å *I* of the north sunspot. The white region is the center of the sunspot, and the black line crosses the north ribbon of the flare, which can be clearly identified in the negative image. Following Isobe et al. (2007), we plot the intensity profiles along the black line during the period from 02:00 UT to 05:00 UT. We find that the reversal effect occurred at 02:28 UT and disappeared at 02:42 UT. This means that the reversal effect lasts for about 14 minutes, which is much shorter than the duration of the flare (about 100 minutes). We show three profiles in Figure 1. Diamonds, stars, and triangles correspond to the profiles at 02:24 UT, 02:28 UT, and 02:42 UT, respectively. Moreover, the first sharp upward variation of the helicity rate in our work occurred around 02:22 UT, which was earlier than the appearance of the reversal effect, and the second sharp downward variation occurred around 04:02 UT, which was much later than the disappearance of the reversal effect. These facts suggest that the reversal effect would obviously not affect our main results. The Stokes *I*, *Q*, *U*, *V* profiles of SP/SOT were recorded at the Fe I 6301.5/6302.5 Å lines. For this AR, SP/SOT data were taken at a duration of 80 minutes with a fast mode. We use two vector magnetograms obtained by this mode to show the configuration of the magnetic field of the AR before and after the major flare. For each vector magnetogram we resolve the 180° ambiguity for the transverse field component by following Wang et al. (2001).

It is well known that the determination of *dH*/*dt* depends on two parameters: the FWHM of the apodizing window and the time interval between two images for comparison. Berger et al. (1998) pointed out that as the FWHM is decreased, the correlation between images becomes dominated by small-scale features that are moving significantly fast. Chae et al. (2004) found that a small window size or a small time interval would result in a larger fluctuation of *dH*/*dt*. Nevertheless, when averaged over a long period, the variation of the average value is less than 10%. Following Chae et al. (2001), we have chosen 8″ for the FWHM for the 96 minute MDI/*SOHO* magnetograms and the same thresholds of the flux density (<10 G) and cross-correlation value (<0.9). NFI/SOT produces magnetograms with a high spatial resolution of 0.16″, on which scale the magnetic field of the penumbra evolves significantly over a few minutes. To enhance the persistent velocity vector, we reduce the spatial resolution of the NFI/SOT magnetograms by using sliding square windows of 0.8″. Then we choose the FWHM as 12.8″/6.4″ and the time interval as 96/6 minutes and the thresholds of the flux density (<10 G)/(<10 G) and cross-correlation value (<0.9)/(<0.8) for both NFI/SOT data sets (0.8″/0.16″). The reason that we used a lower cross-correlation threshold of 0.8 for the high-resolution data is that the high spatial resolution data include more small-scale features, which move fast and evolve rapidly, so the correlation value between two successive images must be relatively low. In order to make the distribution of horizontal velocity with a distribution similar to that of MDI data, we have evaluated the cross-correlation threshold from 0.9 by a step of 0.05 and calculate the corresponding horizontal velocity maps. We find that when we choose 0.8 as the threshold for the high-resolution data, the distribution of the horizontal velocity is very similar to that of MDI data with the cross-correlation threshold as 0.9. It is worth noting that the subregion that we selected to do the Fourier correlation in the LCT method is 20 × 20 pixels, so both cross-correlation values strongly indicate correlation in our sample.

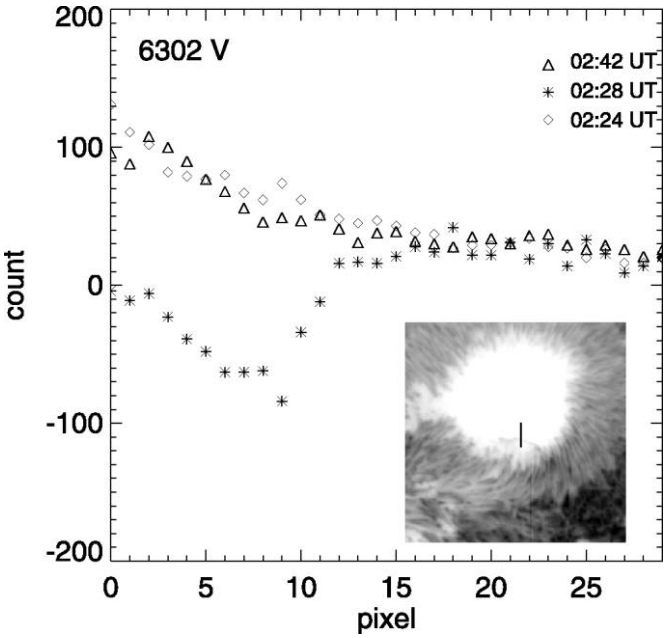

FIG. 1.—Intensity profiles along the black line in the negative 6302 Å *I* image.

In order to show the eruption process, the high-cadence (8 ms) microwave observations at a frequency of 2.84 GHz obtained in SBRS/*Huairou* (Fu et al. 1995, 2004) are used.

3. RESULT OF OBSERVATIONS

Figure 2 shows the SP/SOT vector magnetograms before and after the major flare, which provide the basic magnetic structures of the AR. In this figure, the gray-scale map is the

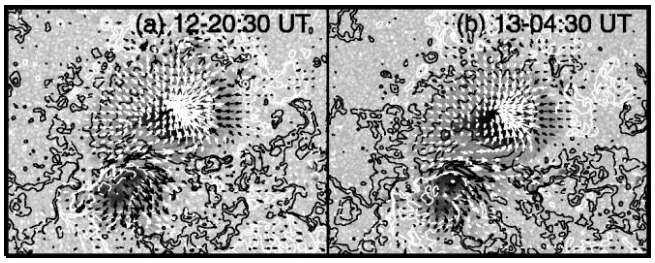

FIG. 2.—Vector magnetograms observed by SP on board *Hinode* at (*a*) 20:30 UT on 2006 December 12 and (*b*) 04:30 UT on 2006 December 13 taken before and after the flare/CME event, respectively. The gray-scale map is the Ca II H image. White (black) contours represent positive (negative) longitudinal magnetic fields. Arrows are the transverse field, and their length is proportional to the field strength. The field of view is $142'' \times 117''$.

Stokes *I* image. White (black) contours represent the positive (negative) longitudinal magnetic field. Arrows are the transverse field, and their length is proportional to the field intensity. From the direction of the transverse field, we find that the north main negative polarity has a slight right-handed twist, and the remains of the AR have a predominantly left-handed twist. The overall twist of the magnetic fields can be measured by $\alpha_{\rm best}$, which is the best-fitting of force-free factor α from the magnetogram (Pevtsov et al. 1995). The whole AR exhibits a negative $\alpha_{\rm best}$ with the value of 1.62×10^{-7} m^{-1} before the flare. The value of $\alpha_{\rm best}$ decreases slightly to 1.48×10^{-7} m^{-1} with the same sign after the flare. This means that the dominant sign of the magnetic helicity in the AR is negative, which is agreeable with the left-handed spiral magnetic field in the south hemisphere. Meanwhile, strong shear is clearly seen in the transverse field along the neutral line. Due to the continuous emergence and eastward motion, the neutral line is dragged almost parallel with the equator.

Figure 3 shows the evolution of horizontal velocity before, during, and after the major flare. The velocity maps are deduced from longitudinal magnetograms. To show the process of the flare clearly, we overlay the velocity map on the Ca II H image at the same time. We can see that the flare occurs in the vicinity of the high sheared neutral line and lasts for a long period. Arrows in this figure represent the distribution of the transverse velocity. We note that the rms value of the speed distribution

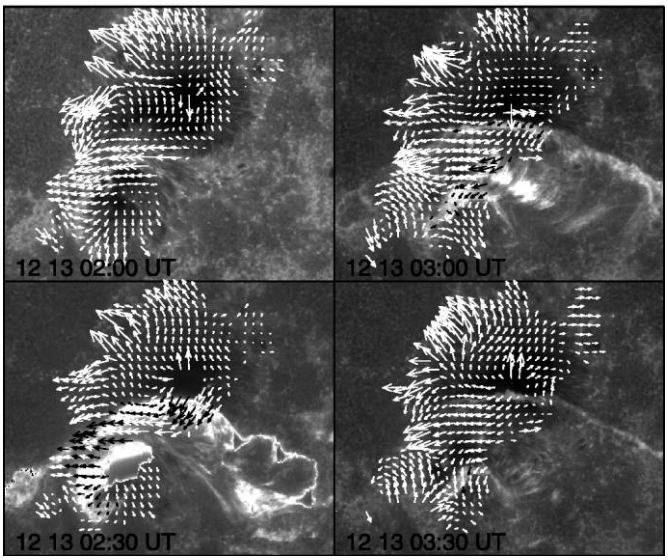

FIG. 3.—Evolution of the horizontal velocity before, during, and after the flare/CME event. The background is the Stokes *I* image, and arrows represent the horizontal velocity. The field of view is $131'' \times 109''$.

is about 0.14 km s^{-1}. This value is much larger than that of solar differential rotation in the same area, which is merely about 0.03 km s^{-1}. From this figure, we find that three kinds of motions persist over the observing hours. The most prominent is a radial expanding motion of the leading sunspots with speed up to about 0.5 km s^{-1}, which is consistent with the result of Chae et al. (2001). Meanwhile, the following sunspot has a rapid counterclockwise (right-handed) rotational motion around its center, which is well consistent with the left-handed transverse magnetic field. The speed of the rotational motion is 0.2–0.4 km s^{-1}. Finally, the shear motion can be seen clearly along the neutral line. It may result from the counterclockwise rotation and eastward motion of the following sunspot, which is responsible for the highly shearing situation of the magnetic field. These three kinds of motions are maintained throughout the flaring time.

Figure 4*a* shows the temporal variation of *dH*/*dt* deduced from MDI during 2006 December 8–14. From the figure, we

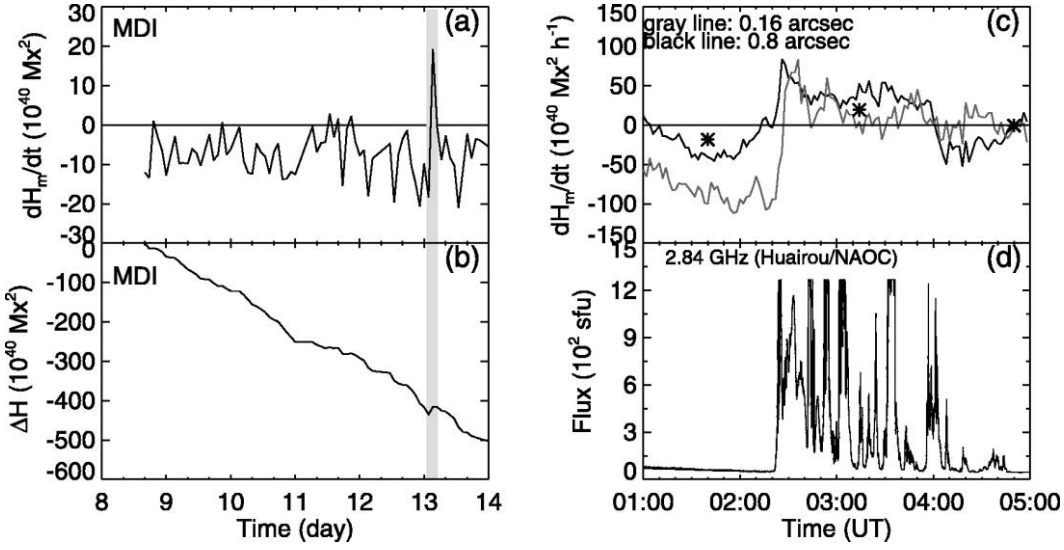

FIG. 4.—(*a*) Long-term evolution of the transport rate of magnetic helicity during 2006 December 8–14. (*b*) Accumulated magnetic helicity as a function of time. (*c*) Profiles of the rate of magnetic helicity around the flaring time. (*d*) Microwave emission flux at a frequency of 2.84 GHz observed at SBRS/*Huairou*.

first see that the transport rate of magnetic helicity is predominantly negative throughout the observing period. This implies that the accumulation of the magnetic helicity is negative, which is consistent with the sign of magnetic helicity inferred from vector magnetograms. The figure further shows that there is a sharp variation of *dH*/*dt* during the period of the major flare between 01:36 UT and 04:30 UT. It can be seen clearly that the sign of *dH*/*dt* changes from negative to positive and then from positive to negative (marked by shadow area in the figure). This means that during the flaring time, the magnetic helicity with positive sign was impulsively injected into the corona. This variation can also be found from the accumulated magnetic helicity (Fig. 4*b*), which was obtained by integrating the measured *dH*/*dt* from the start of the observing run to the specified time. As the sign of *dH*/*dt* changes, the accumulated magnetic helicity decreases slightly.

However, with the low temporal resolution of 96 minute MDI full-disk magnetograms, we get only one data point during the flaring time that reflects the sharp variation of *dH*/*dt*. In order to reveal the details around the sharp variation, we do the same calculation using the high temporal resolution data from NFI/SOT with 2 minute intervals. The time period (01:00–05:00 UT) we calculated is marked with a shadow area in Figures 4*a* and 4*b*. The detailed temporal variation of *dH*/*dt* is shown in Figure 4*c* by the solid lines (black for 0.8″ and gray for 0.16″). Stars represent the values obtained from MDI data. A horizontal line outlines the zero value of *dH*/*dt*. Figure 4*c* shows that the sharp variation of *dH*/*dt* does exist. Here, we present the profile of the microwave emission flux at a frequency of 2.84 GHz observed by NAOC/*Huairou* in Figure 4*d*. Compared to Figures 4*c* and 4*d*, we find that the sign of *dH*/*dt* changes from negative to positive around the start of the eruption, and then drops rapidly back to its initial status with negative sign around the eruption end. During the flaring time of about 100 minutes, positive magnetic helicity was impulsively injected into the corona through the photosphere. Moreover, the variation tendencies of MDI and NFI/SOT data are almost the same. We also note that the absolute value of *dH*/*dt* deduced from the high spatial resolution data is larger than that from the low spatial resolution data before the flare. After the flare, the behavior becomes the reverse. The possible reason may be that the small-scale motions of some fine structures that can be identified only in high spatial resolution data contribute to the accumulation of magnetic helicity. The nature of these fine structures and their contribution to the magnetic helicity accumulation deserve further investigation.

4. DISCUSSION AND CONCLUSION

In this work, we identify a close relationship between the sharp variation of *dH*/*dt* and a microwave burst (i.e., a major flare) that took place in AR 10930. Moreover, the most interesting point is that, in our work, the temporal variation of *dH*/*dt* is consistent with a microwave burst at a frequency of 2.84 GHz. We know that a microwave burst is a prompt signal of nonthermal energetic particles originating from the magnetic reconnection during the impulsive phase of a solar flare, which may reveal the mechanisms of magnetic energy release and particle acceleration. On the other hand, magnetic helicity is a measure of the twist and linkage of magnetic field lines (DeVore 2000), which may change immediately after the magnetic reconnection. The strong correlation between them may shed some light on the flaring processes associated with energy release during the magnetic reconnection.

The study of the relationship between magnetic helicity transport and solar eruption is essential in understanding the energy release and magnetic reconfiguration processes. Using the high temporal resolution data of NFI/SOT, we study the variation of *dH*/*dt* in AR 10930 during an X3.4/4B flare/CME event. The AR is a dominant and unique one on the solar disk when the flare took place. These imply that the variation of *dH*/*dt* that resulted from the field lines passing through the side boundary can be neglected. Here, we find that the sharp variations of *dH*/*dt* are strongly consistent with a microwave burst at a frequency of 2.84 GHz. Around the onset of the flare, the variation of *dH*/*dt* changes its sign from negative to positive. And near the end of the flare it goes back to its original sign. That is, during the flaring time, magnetic helicity with positive sign was impulsively injected into the corona. Our observational results suggest that the transport of magnetic helicity may play an important role in the process of solar eruptions.

We thank the anonymous referee, whose comments and suggestions have improved the quality of this Letter. We are grateful to the *Hinode*, SBRS, and MDI teams for providing the wonderful data. This work was supported by the National Basic Research Program of MOST (grant 2006CB806301), NSFC grants 10333030 and 10733020, and the CAS-NSFC Key Project (grant 10778605). *Hinode* is a Japanese mission developed and launched by ISAS/JAXA, with NAOJ as domestic partner and NASA and STFC (UK) as international partners. It is operated by these agencies in cooperation with ESA and NSC (Norway).

REFERENCES

Bao, S., & Zhang, H. 1998, ApJ, 496, L43
Berger, M. A., & Field, G. B. 1984, J. Fluid Mech., 147, 133
Berger, T. E., & Lites, B. W. 2003, Sol. Phys., 213, 213
Berger, T. E., Loefdahl, M. G., Shine, R. S., & Title, A. M. 1998, ApJ, 495, 973
Chae, J., Moon, Y. J., & Park, Y. D. 2004, Sol. Phys., 223, 39
Chae, J., Wang, H. M., Qiu, J., Goode, P. R., Strous, L., & Yun, H. S. 2001, ApJ, 560, 476
Chae, J., et al. 2007, PASJ, 59, S619
Démoulin, P., & Berger, M. A. 2003, Sol. Phys., 215, 203
Deng, Y. Y., Wang, J. X., Yan, Y. H., & Zhang, J. 2001, Sol. Phys., 204, 11
DeVore, C. R. 2000, ApJ, 539, 944
Fu, Q. J., Qin, Z. H., Ji, H., & Pei, L. 1995, Sol. Phys., 160, 97
Fu, Q. J., et al. 2004, Sol. Phys., 222, 167
Hartkorn, K., & Wang, H. M. 2004, Sol. Phys., 225, 311
Isobe, H., et al. 2007, PASJ, 59, S807
Kosugi, T., et al. 2007, Sol. Phys., 243, 3
Leka, K. D., Canfield, R. C., & McClyment, A. N. 1996, ApJ, 462, 547
Lin, Y., & Gaizauskas, V. 1987, Sol. Phys., 109, 81
Maeshiro, T., Kusano, K., Yokoyama, T., & Sakurai, T. 2005, ApJ, 620, 1069
Moon, Y. J., Chae, J. Y., Choe, G. S., Wang, H. M., Park, Y. D., Yun, H. S., Yurchyshyn, V., & Goode, P. R. 2002a, ApJ, 574, 1066
Moon, Y. J., Chae, J. Y., & Park, Y. D. 2003, J. Korean Astron. Soc., 36, S37
Moon, Y. J., Chae, J. Y., Wang, H. M., Choe, G. S., & Park, Y. D. 2002b, ApJ, 580, 528
Nindos, A., Zhang, J., & Zhang, H. Q. 2003, ApJ, 594, 1033
November, L. J., & Simon, G. W. 1988, ApJ, 333, 427
Pevtsov, A. A., Canfield, R. C., & Metcalf, T. R. 1995, ApJ, 440, L109
Qiu, J., & Gary, D. E. 2003, ApJ, 599, 615
Tan, B. L., Ji, H. S., Huang, G. L., Zhou, T. H., Song, Q. W., & Huang, Y. 2006, Sol. Phys., 239, 137
Tsuneta, S., et al. 2008, Sol. Phys., 249, 167
Wang, H. M., Qiu, J., Spirock, T. J., Yurchyshyn, V., Abramenko, V., Ji, H., & Goode, P. R. 2004, ApJ, 605, 931
Wang, H. N., Yan, Y. H., & Sakurai, T. 2001, Sol. Phys., 201, 323
Zhang, J., Li, L. P., & Song, Q. 2007, ApJ, 662, L35